

HIGH SPATIAL RESOLUTION OBSERVATIONS OF LOOPS IN THE SOLAR CORONA

DAVID H. BROOKS^{1,4}, HARRY P. WARREN², IGNACIO UGARTE-URRA¹, AMY R. WINEBARGER³

¹College of Science, George Mason University, 4400 University Drive, Fairfax, VA 22030

²Space Science Division, Naval Research Laboratory, Washington, DC 20375 and

³NASA Marshall Space Flight Center, ZP 13, Huntsville, AL 35812

Draft version January 27, 2023

ABSTRACT

Understanding how the solar corona is structured is of fundamental importance to determining how the Sun's upper atmosphere is heated to high temperatures. Recent spectroscopic studies have suggested that an instrument with a spatial resolution of 200 km or better is necessary to resolve coronal loops. The *High Resolution Coronal Imager (Hi-C)* achieved this performance on a rocket flight in July 2012. We use *Hi-C* data to measure the Gaussian widths of 91 loops observed in the solar corona and find a distribution that peaks at about 270 km. We also use *Atmospheric Imaging Assembly (AIA)* data for a subset of these loops and find temperature distributions that are generally very narrow. These observations provide further evidence that loops in the solar corona are often structured at a scale of several hundred kilometers, well above the spatial scale of many proposed physical mechanisms.

Keywords: Sun: corona—Sun: UV radiation—magnetic fields

1. INTRODUCTION

Spatial resolution plays a critical role in interpreting observations of the solar corona. At very low spatial resolution (~ 5000 km) it is clear that many independent structures are being observed along the line of sight and any attempt to model such observations must account for this superposition. An important question in solar physics is at what spatial scale do we begin to observe isothermal structures that evolve on timescales comparable to a radiative cooling time. Some mechanisms that are thought to be responsible for the heating of the solar corona are expected to operate at very small spatial scales. For example, many numerical simulations of magnetic reconnection (e.g. Shay et al. 2001) suggest that current sheets form on the scale of the ion inertial length ($d_i = c/\omega_{pi}$), which is on the order of several hundred meters in the solar corona. This would suggest that the observation of resolved coronal loops may not be achieved for the foreseeable future.

There is some evidence, however, that coronal loops are actually structured at much larger spatial scales. Some of the highest spatial resolution observations of the solar corona obtained on a routine basis have been from the *Transition Region and Coronal Explorer* (Handy et al. 1999). Analysis of million degree loop structures observed by *TRACE* in the Fe IX 171 Å channel yielded a mean width and standard deviation of 1400 ± 300 km for the distribution (Aschwanden & Nightingale 2005). This was higher than the instrumental point spread function of about 900 km and suggested that loops might actually be resolved at this spatial resolution. Furthermore, spectroscopic observations have indicated that the temperature distributions in these loops are often very narrow (Del Zanna 2003; Warren et al. 2008), consistent with the interpretation that loops at coronal temperatures are, or are close to being, resolved.

The temporal evolution of loops observed at million degree temperatures provides additional insights into the structuring of the corona. Observations often show loops

that appear in progressively lower ionization stages over time, suggesting that they are cooling (e.g. Winebarger et al. 2003; Ugarte-Urra et al. 2009; Mulu-Moore et al. 2011; Viall & Klimchuk 2011). Numerical simulations of this evolution, however, indicate that the loops evolve on time scales much longer than a radiative cooling time, suggesting that they may consist of at least a few unresolved strands (Reale & Peres 2000; Warren et al. 2003). Brooks et al. (2012) used densities measured from relatively low spatial resolution spectroscopic observations to infer the actual emitting volume in coronal loops. They found that the observed emission could be reproduced with only a small number of sub-resolution threads several hundred kilometers in width.

Observations at optical wavelengths also suggest that coronal loops are structured on scales below 1000 km but above the very small spatial scale of many proposed physical mechanisms. For example, the observation of coronal condensations, which form when coronal plasma cools catastrophically to very low temperatures and falls back to the surface of the Sun, suggests that coronal loops have widths of a few hundred km (Antolin & Rouppe van der Voort 2012). The low temperatures of the condensations allow them to be imaged at very high spatial resolution by optical telescopes. The diffraction limit of the CRisp Imaging SpectroPolarimeter (CRISP) used for these coronal rain observations is approximately 100 km (Scharmer et al. 2008). Antolin & Rouppe van der Voort (2012) also reported condensations forming nearly simultaneously on adjacent field lines, consistent with the idea that heating is coherent across several threads over larger scales in the corona.

The launch of the *High Resolution Coronal Imager (Hi-C)* on a sub-orbital rocket flight has provided a new opportunity to observe the spatial structuring of the solar corona directly (Cirtain et al. 2013). *Hi-C* observed a bandpass dominated by the Fe XII 195.119 Å line with a spatial resolution of about 150 km, possibly sufficient to resolve loops. In this paper we examine loop cross sections for a sample of coronal loops observed with *Hi-C* and find a distribution of Gaussian widths that peaks at about 270 km. These observations provide convincing evidence that the solar corona is structured at a scale

⁴ Current address: Hinode Team, ISAS/JAXA, 3-1-1 Yoshinodai, Chuo-ku, Sagami-hara, Kanagawa 252-5210, Japan

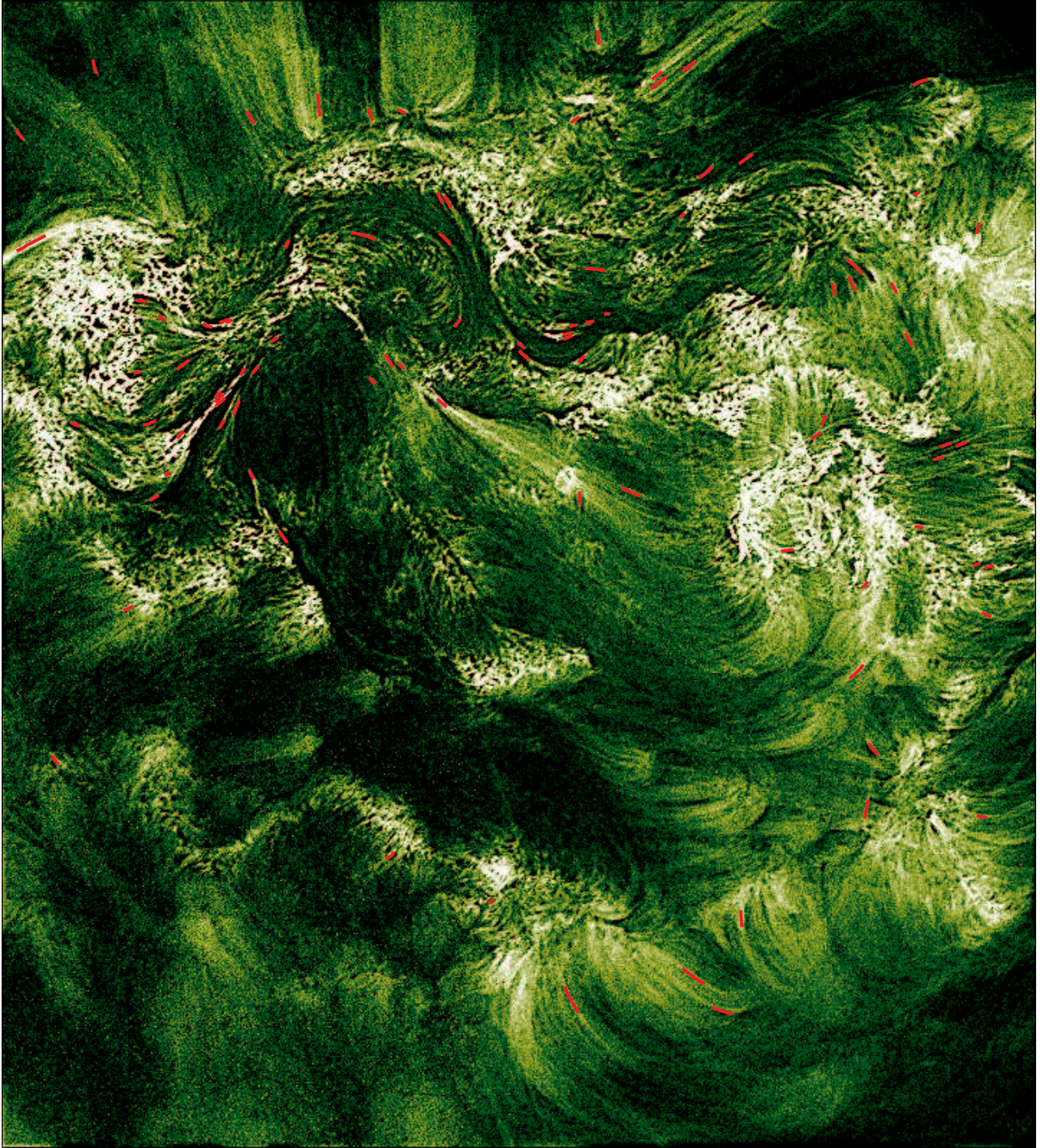


Figure 1. *Hi-C* image of AR 11520/11521 taken at 18:55:30UT on 2012, July 11. The 91 loop segments are marked in red. The image in this figure has been treated with a Gaussian sharpening filter to highlight the fine structure.

of several hundred kilometers, suggesting that coronal loops may be routinely resolved by the next generation of solar instrumentation.

2. OBSERVATIONS AND ANALYSIS METHODS

The *Hi-C* instrument comprises a CCD camera and Ritchey-Chretien telescope that observes in a 5 \AA wide band-pass around 193 \AA . It was flown on 2012 July 11, and obtained images of the solar corona at the highest spatial resolution ever achieved. Details of the instrument are given by Cirtain et al. (2013), who indicate that the spatial resolution

was close to $0.2''$ (or about 150 km). The target of the flight was the active region complex designated 11520/11521. We obtained the data pre-processed from the Virtual Solar Observatory. They are full resolution level 1.5 data and have had the dark current subtracted. They have also been cropped, flat-fielded, normalized, unrolled, internally coaligned, and cleaned of dust. We also coaligned them to near simultaneous full Sun 193 \AA images from the *Atmospheric Imaging Assembly* (AIA, Lemen et al. 2012) on the *Solar Dynamic Observatory* (SDO, Pesnell et al. 2012).

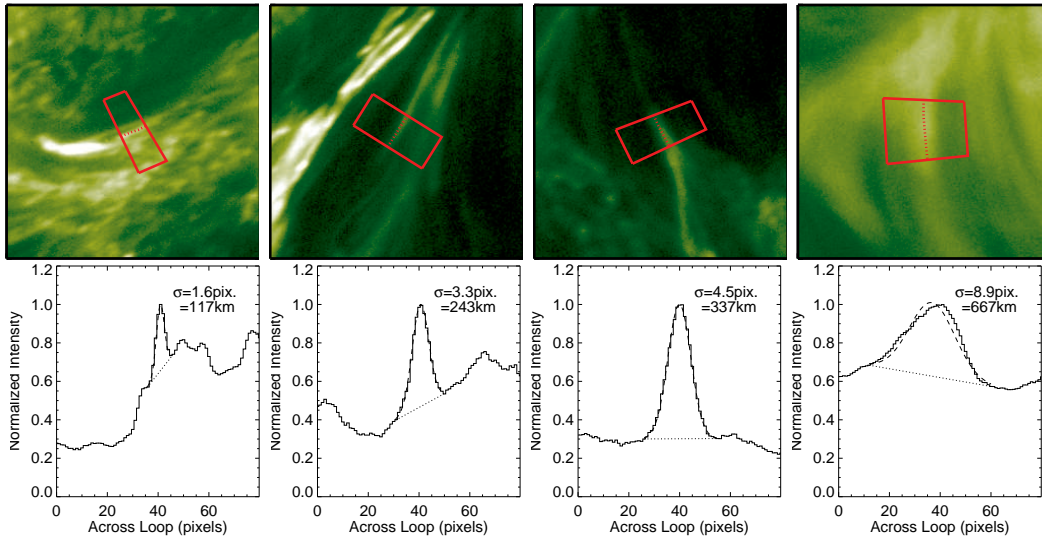


Figure 2. Example loop segments. Top row: *Hi-C* images with the loop segments highlighted in red. Bottom row: cross loop normalized intensity profiles (solid histogram) with Gaussian fits (dash) and backgrounds (dot) overlaid. The Gaussian width in *Hi-C* pixels and *km* is indicated in the legend. The interpolated data have been resampled to show the instrument pixel scale.

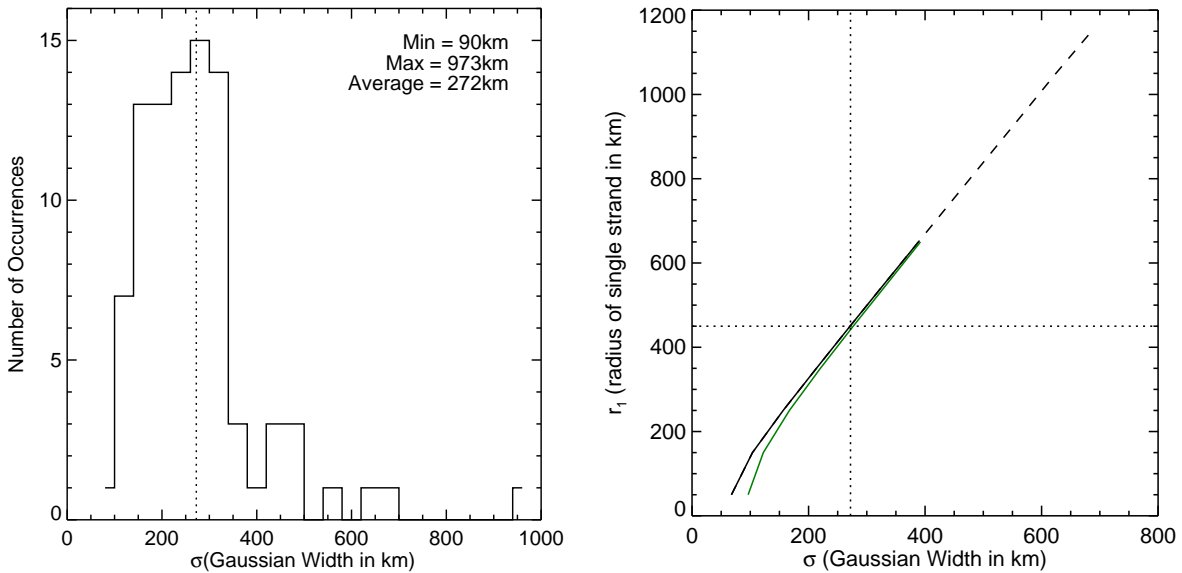


Figure 3. Left panel: distribution of Gaussian widths measured for the sample of 91 loop segments shown in Figures 1 and 2. Right panel: relationship between the true loop radius and the simulated *Hi-C* measured Gaussian width if the loop consists of a single strand. As the radius becomes much larger than the PSF of the instrument, the Gaussian shape becomes a poorer fit to the loop cross-section (dashed line). Black and green lines represent a PSF of 0.2'' and 0.3'', respectively.

An example *Hi-C* image taken at 18:55:30UT is shown in Figure 1. The image has been treated with a Gaussian sharpening filter to highlight the fine structure. This filter was only applied for presentation, all the analysis was performed on the original data. We visually identified a number of loops in the 18:55:30UT image. Our sample does not cover every loop-like feature in the image, and there is likely to be a selection bias towards loops that are distinctive and have relatively pronounced cross-loop intensity profiles. Nevertheless, we were able to identify 91 loop-like segments and they are marked in red. Following Aschwanden et al. (2008) and

Warren et al. (2008), we extracted cross-loop intensity profiles by interpolating along the axis of the loop, straightening it, and averaging the intensities along the selected segment. We then selected two background positions in the intensity profile and fit them with a first order polynomial. A Gaussian function is then fitted to the background subtracted intensity profile and the Gaussian width is taken as our measurement. Several examples are shown in Figure 2.

Many of these loops are also visible in the *AIA* images. We extracted co-spatial cross loop intensity profiles from the coaligned *AIA* images and found that 79 of the *AIA* 193 Å

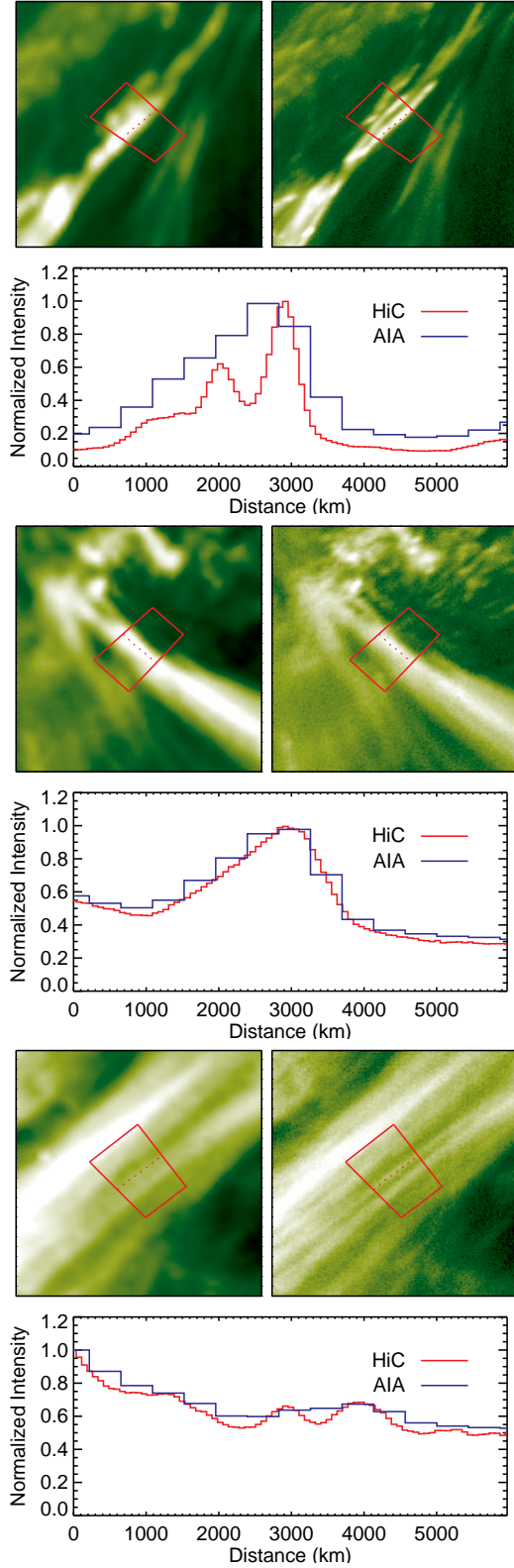


Figure 4. *Hi-C* and *AIA* images and intensity profiles. Top panel: Example of a loop segment that is apparently composed of 1-2 structures when imaged by *AIA*, but is revealed by *Hi-C* to consist of at least 3 structures. Middle panel: Example of a loop segment that appears to be a single structure when imaged by either instrument. Bottom panel: Example of a relatively long loop that shows substructure in *Hi-C*.

profiles are highly correlated ($C > 0.8$) with those of *Hi-C*, allowing us to perform an emission measure (EM) analysis of the loops using the *AIA* filters. We therefore extracted the intensities from all the filters by fitting a Gaussian to the cross-loop *AIA* profiles using the *Hi-C* defined background positions. We then fit a Gaussian EM to the *AIA* intensities, assuming an uncertainty of 25% (Boerner et al. 2012). Only the intensities of highly correlated filter profiles are used in the analysis, though we relax the condition a little ($C > 0.7$) to allow for any residual offsets in the coaligned data (as discussed by Aschwanden & Boerner 2011). The other intensities are set to zero, and we also set the 94 \AA intensity to zero. This step is necessary to provide a high temperature constraint on the EM, which has relatively large uncertainties due to poor temperature fidelity and coarse coverage. We assume that the emission measure distribution is a Gaussian

$$\xi(T) = \frac{EM_0}{\sigma_T \sqrt{2\pi}} \exp \left[-\frac{(T - T_0)^2}{2\sigma_T^2} \right], \quad (1)$$

and use a least-squares approach to determine the best-fit total emission measure (EM_0), peak temperature (T_0), and thermal width (σ_T).

3. RESULTS AND DISCUSSION

The distribution of Gaussian loop widths for the entire sample of 91 loop segments is shown in Figure 3. The values range from 90–1000 km. The minimum measurement of 90 km translates to a 212 km FWHM, which is about $0.12''$. This is close to the laboratory performance of *Hi-C* (Cirtain et al. 2013). López Fuentes et al. (2006) and Brooks et al. (2012) have pointed out that there is a complex relationship between measured loop widths and the actual loop radius that depends on the instrument characteristics. This makes it difficult to accurately infer the physical width from the measured width. Our view is that the best approach is to construct physical models of the emission, convolve them with the instrument parameters, and compare the results with the observations. To illustrate this we assume that a loop consists of a single strand at a temperature of 1.6 MK and density of $\log N = 9$ and that the plate scale is $0.07''$ and the width of the point spread function is $0.2''$ (FWHM, Cirtain et al. 2013; Kobayashi 2013). As is shown in Figure 3, with these assumptions, the mean value of the distribution (272 km) corresponds to a loop radius (~ 450 km); a value close to the mean of the loop sample analyzed by Brooks et al. (2012).

Figure 4 contrasts the *AIA* view of three of the loop segments with the same region observed by *Hi-C*. The loop in the top panel appears to be composed of a dominant bright structure and another nearby that is not spatially separated nor fully distinct in the cross-loop intensity profile. Not only does *Hi-C* begin to separate these structures, but it reveals the presence of a third.

It is tempting to conjecture from these examples that moving to higher spatial resolution will always reveal new substructure, as expected on theoretical grounds. This behavior, however, is very similar to that reported by Brooks et al. (2012) when comparing *AIA* data with lower spatial resolution observations from the EUV Imaging Spectrometer (*EIS*, Culhane et al. 2007) on *Hinode*. They argued that the observation of resolved loops, and *EIS* structures that appear to separate out spatially into individual loops when imaged by *AIA*, could mean that the spatial scales of loops are not far below the resolutions of those instruments. In

turn suggesting a topologically simple corona or that magnetic braiding takes place on unexpectedly large spatial scales. The latter interpretation has been independently suggested by Cirtain et al. (2013), who claim to have observed spatially resolved magnetic braids for the first time with *Hi-C*. Note that the loop segment in Figure 4 is the same example as shown by Cirtain et al. (2013).

Even at the modest spatial resolution of *EIS* (1800 km FWHM PSF) some loops appear to be resolved (Brooks et al. 2012). This indicates that some of the loops observed by *TRACE* were probably also resolved, as suggested by Aschwanden & Nightingale (2005). Though the latter could not be unambiguously confirmed because of a lack of spectroscopic diagnostics (densities). Since *Hi-C* is also an imager, we cannot confirm this here. We do, however, find clear cases of relatively large loops observed by *AIA* that look almost identical at the higher spatial resolution of *Hi-C*. An example is shown in the middle panel of Figure 4. This loop has a Gaussian width of 554 km in *AIA* and 562 km when measured by *Hi-C*. As discussed, many coronal loops observed spectroscopically at lower spatial resolution have been found to have narrow temperature distributions. These loops likely correspond to examples of large loops observed by *Hi-C* like this one. From our EM analysis we found that this loop has a narrow thermal width of $\sigma_T=0.32$ MK.

Nevertheless, the thermal width of even this loop is larger than the majority of the loops in the sample. The loop in the top panel of Figure 4, for example, has a thermal width of $\sigma_T=0.04$ MK. From our EM analysis of the complete sample of all the loops detectable with *AIA*, we found that 70% have $\sigma_T \lesssim 0.32$ MK. These results are comparable to spectroscopic measurements by *EIS* (Warren et al. 2008), though there are relatively more loops with a broad temperature distribution, reflecting the larger uncertainties in the *AIA* EM analysis. The results do, however, support the idea that these loops have narrow temperature distributions and are composed of only a few magnetic threads.

Recently Peter et al. (2013) analyzed several long loops observed by *Hi-C* and found that they have smooth cross-field intensity profiles. They suggested that they are either single monolithic structures or are composed of many very small strands. With our larger sampling of the data we do in fact find some cases of long loops that show evidence of substructure when imaged by *Hi-C*. The loop shown in the bottom panel of Figure 4 is the best example. The results for these loops are not atypical. The widths of loops like this fall within the distribution of Figure 3. We do agree with the conclusion of Peter et al. (2013) that many of the narrow features within the *Hi-C* field of view appear to be relatively short loops.

The instrument performance achieved by the *Hi-C* team demonstrates that 100 km spatial scales will be routinely observable with future coronal spectrometers such as that

planned for *Solar-C* (Teriaca et al. 2012). The results presented here are encouraging to the view that such instruments will be able to measure the true plasma properties of coronal loops, and provide realistic constraints for coronal heating models. If confirmed by these instruments, then our *Hi-C* loop width measurements already represent the true spatial scales of coronal structures. Theoretical models need to explain why the corona is structured on these scales, and why the temperature distributions are narrow over scales of hundreds of km.

We acknowledge the High resolution Coronal Imager instrument team for making the flight data publicly available. MSFC/NASA led the mission and partners include the Smithsonian Astrophysical Observatory in Cambridge, Massachusetts; Lockheed Martin's Solar Astrophysical Laboratory in Palo Alto, California; the University of Central Lancashire in Lancashire, England; and the Lebedev Physical Institute of the Russian Academy of Sciences in Moscow. This work was performed under contract with the Naval Research Laboratory and was funded by the NASA *Hinode* program. *Hinode* is a Japanese mission developed and launched by ISAS/JAXA, with NAOJ as domestic partner and NASA and STFC (UK) as international partners. It is operated by these agencies in co-operation with ESA and NSC (Norway).

REFERENCES

- Antolin, P., & Rouppe van der Voort, L. 2012, *ApJ*, 745, 152
 Aschwanden, M. J., & Boerner, P. 2011, *ApJ*, 732, 81
 Aschwanden, M. J., & Nightingale, R. W. 2005, *ApJ*, 633, 499
 Aschwanden, M. J., Nitta, N. V., Wuelsel, J., & Lemen, J. R. 2008, *ApJ*, 680, 1477
 Boerner, P., et al. 2012, *Sol. Phys.*, 275, 41
 Brooks, D. H., Warren, H. P., & Ugarte-Urra, I. 2012, *ApJ*, 755, L33
 Cirtain, J. W., et al. 2013, *Nature*, 493, 501
 Culhane, J. L., et al. 2007, *Sol. Phys.*, 243, 19
 Del Zanna, G. 2003, *A&A*, 406, L5
 Handy, B. N., et al. 1999, *Sol. Phys.*, 187, 229
 Kobayashi, K. 2013, *Sol. Phys.*, submitted
 Lemen, J. R., et al. 2012, *Sol. Phys.*, 275, 17
 López Fuentes, M. C., Klimchuk, J. A., & Démoulin, P. 2006, *ApJ*, 639, 459
 Mulu-Moore, F. M., Winebarger, A. R., Warren, H. P., & Aschwanden, M. J. 2011, *ApJ*, 733, 59
 Pesnell, W. D., Thompson, B. J., & Chamberlin, P. C. 2012, *Sol. Phys.*, 275, 3
 Peter, H., et al. 2013, *A&A*, *in press*
 Reale, F., & Peres, G. 2000, *ApJ*, 528, L45
 Scharmer, G. B., et al. 2008, *ApJ*, 689, L69
 Shay, M. A., Drake, J. F., Rogers, B. N., & Denton, R. E. 2001, *J. Geophys. Res.*, 106, 3759
 Teriaca, L., et al. 2012, *Experimental Astronomy*, 34, 273
 Ugarte-Urra, I., Warren, H. P., & Brooks, D. H. 2009, *ApJ*, 695, 642
 Viall, N. M., & Klimchuk, J. A. 2011, *ApJ*, 738, 24
 Warren, H. P., Ugarte-Urra, I., Doschek, G. A., Brooks, D. H., & Williams, D. R. 2008, *ApJ*, 686, L131
 Warren, H. P., Winebarger, A. R., & Mariska, J. T. 2003, *ApJ*, 593, 1174
 Winebarger, A. R., Warren, H. P., & Seaton, D. B. 2003, *ApJ*, 593, 1164